In situ x-ray reflectivity study of the oxidation kinetics of liquid gallium and the liquid alloy $Ga_{0.93}Hg_{0.07}$

1998 J. Phys.: Condens. Matter 10 971

(http://iopscience.iop.org/0953-8984/10/5/007)

J. Phys.: Condens. Matter **10** (1998) 971–982. Printed in the UK PII: S0953-8984(98)88718-3

In situ x-ray reflectivity study of the oxidation kinetics of liquid gallium and the liquid alloy $Ga_{0.93}Hg_{0.07}$

Anton Plech, Uwe Klemradt†, Hartmut Metzger and Johann Peisl
Sektion Physik der LMU München, Geschwister-Scholl-Platz 1, D-80539 München, Germany

Received 27 October 1997

Abstract. The low-temperature oxidation kinetics of liquid Ga and the liquid alloy $Ga_{0.93}Hg_{0.07}$ has been investigated by means of *in situ* x-ray specular reflectivity. A combination of angle-dispersive and energy-dispersive measurements was used to obtain a time resolution of 20 minutes with a sealed-tube reflectometer, allowing us to follow the growth of a natural oxide layer for 1 to 170 hours following preparation of a fresh surface. Oxide layer thicknesses between 10 and 30 Å were measured for Ga at 103 °C and the liquid alloy at 83 °C, 107 °C and 122 °C. The oxidation was found to follow a logarithmic growth law in all cases.

1. Introduction

The study of oxidation processes is a well-established field in materials research due to the importance of corrosion in metallurgy and the vital properties of SiO_2 in semiconductor technology. A large body of theoretical work has been amassed especially on metal oxidation. Depending on the assumptions for the rate-limiting physical process, different time laws have been published for the growth of an oxide layer, e.g. the well-known parabolic law, by Wagner [1], and logarithmic and inverse-logarithmic laws, by Mott and Cabrera [2–4] and Uhlig [5]. Fromhold and Cook [6, 7] combined several mechanisms in a generalized growth law by including coupled currents of mass and charge transport through the oxide, which reveals large deviations from the classical laws in the primary state of oxidation.

Up to now, there have been very few experimental data available on the oxidation of liquid metals because of numerous experimental difficulties, in spite of the importance of liquid metal interfaces for various metal-forming processes. In a recent study, Salas *et al* [8] reported on inhomogeneous oxide layers produced by the oxidation of liquid aluminium alloys at higher temperatures. Stoneman and MacKay [9] found logarithmic oxidation behaviour for liquid eutectic Pb–Sn in a temperature range of 200 to 460 °C. The reactivity of a liquid metal surface, manifested by a relatively high surface tension, can alter rather drastically the oxidation process, which can result in a different growth law, as recently demonstrated for In–Sn, where logarithmic oxidation behaviour was found for solid In–Sn and parabolic oxidation for liquid In–Sn [10].

The system Ga–Hg is a very promising candidate for the experimental study of phase transitions and wetting phenomena in binary metallic mixtures due to its low critical point at 204 °C [11]. To our knowledge, the oxidation of Ga–Hg has not been investigated yet

† Present address: Physics Department, University of Houston, 4800 Calhoun Road, Houston, TX 77204-5506, USA.

0953-8984/98/050971+12$19.50

experimentally, although oxidation processes at liquid Ga surfaces have been addressed recently [12–15]. In this work we present an *in situ* study of the formation of very thin natural oxide layers on liquid Ga and $Ga_{0.93}Hg_{0.07}$. The low growth temperatures, near 100 °C, result in oxide thicknesses below 40 Å, which are very interesting because they represent the initial stage of oxidation, where it is unclear how far theories well established for thicker films are valid and give the correct growth law [16].

Oxide thicknesses have been determined by specular x-ray reflectivity. This non-destructive technique, widely used in surface and thin-film analysis [17, 18], allows an accurate quantification of surface and interface roughness and—in contrast to other techniques—an independent determination of film densities and thicknesses, as the index of refraction for x-rays is extremely close to unity. X-ray reflectometry is well suited for studying oxidation processes on the nm scale as is evident from previous investigations, e.g. with regard to the corrosion of thin epitaxial Fe films [19] and the formation of oxide layers on liquid Ga by controlled oxygen dosage [15]. Although reflectivity experiments are typically performed in an angle-dispersive (AD) set-up, it should be emphasized that energy-dispersive (ED) measurements—using a wide range of wavelengths at a fixed angle of incidence—are very advantageous in many experimental situations. AD measurements can be performed very quickly for the high fluxes of the total reflection regime and provide intensity data that can be scaled easily to absolute reflectivity units, whereas ED measurements allow fast data collection for higher momentum transfer without the need for moving the sample. As this is especially suited to the investigation of time-dependent phenomena and liquids, we used a combination of AD and ED reflectivity measurements to take advantage of the relative merits of both experimental techniques.

2. Theory

Grazing-angle x-ray reflectivity can be described in terms of classical optics if the appropriate index of refraction n is used in Fresnel's equations [20]. For x-rays, $n = 1 - \delta$ with

$$\delta = \frac{r_0}{2\pi}\lambda^2\rho_e \tag{1}$$

where $r_0 = 2.818 \times 10^{-15}$ m denotes the classical electron radius, λ the x-ray wavelength and ρ_e the electron density of the material under investigation (for dispersion and absorption corrections see [20, 21]). As n is less than unity, total external reflection occurs for x-rays incident below a critical angle $\alpha_c = \sqrt{2\delta}$, which is typically a few tenths of a degree. For $\alpha \gg \alpha_c$ the Fresnel reflectivity drops quickly with $R_F \sim \alpha^{-4}$. Except for the vicinity of absorption edges, the reflectivity can be expressed as a function of just the absolute value of the scattering vector $Q = (4\pi/\lambda)\sin\alpha$, demonstrating formally the equivalence of ED and AD measurements if they are performed under experimental conditions where dispersion effects are negligible.

The information content of reflectivity experiments is the laterally averaged electron density profile along the surface normal, denoted in the following as the z-direction. Within a kinematical approach, the measured reflectivity is related to the Fresnel reflectivity R_F of an ideal surface by the Fourier transform of the derivative of the averaged electron density profile [22, 18]:

$$\frac{R}{R_F} = \left| \frac{1}{\rho_{Bulk}} \int \frac{\mathrm{d}\langle\rho(z)\rangle}{\mathrm{d}z} \mathrm{e}^{\mathrm{i}Qz}\, \mathrm{d}z \right|^2. \tag{2}$$

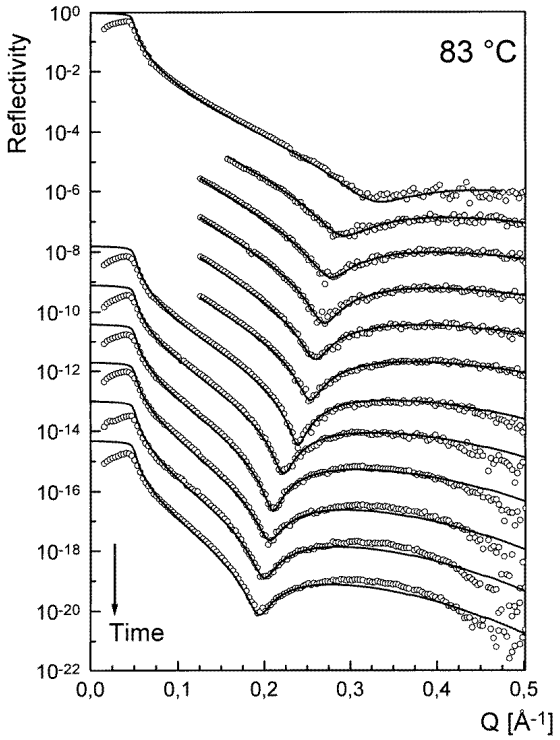

Figure 1. Reflectivities observed for the oxidation of $Ga_{0.93}Hg_{0.07}$. The curve at the top shows the data obtained at room temperature; the lower ones refer to successive times after rapid heating to $T = 83$ °C. The curves are displaced for clarity. Fits to the data are represented by solid lines.

Therefore reflectivity experiments are very sensitive to electron gradients due to surface and interface roughness. Furthermore, equation (2) indicates that a finite jump in the electron density, e.g. caused by an oxide layer, leads to reflectivity oscillations, the frequency of which allows one to determine the layer thickness.

However, to include also data close to the total reflection regime in our analysis, we used a generalized Parratt algorithm [23] for simulations, taking into account properly multiple reflections, dispersion and absorption corrections. The root mean square (RMS) roughness of the surface and the oxide–liquid interface was included according to Névot and Croce [24].

3. Experimental details

The reflectometer consisted of a 3 kW sealed molybdenum tube operated at 50 kV, slits and a sample holder which allowed vertical motion to select a reflection angle from the divergent white beam emitted by the target. Details are described elsewhere [25]. A liquid-nitrogen-cooled intrinsic Ge crystal was used as an energy-dispersive detector with a resolution of 200 to 300 eV at energies between 5 and 45 keV and a dynamic range of 10^5. For AD measurements the detector was operated in a quasi-monochromatic mode by recording only energy channels corresponding to Mo Kα radiation, whereas for ED measurements the

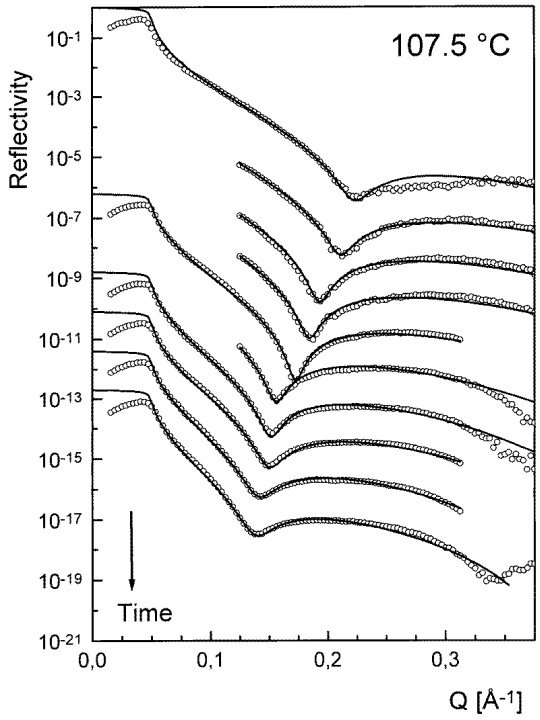

Figure 2. As for figure 1, but for $T = 107.5$ °C.

full spectrum of the multichannel analyser was used, with photons between 5 and 45 keV detected simultaneously. The limitations arise from the absorption of x-ray windows and the tube characteristics, which had to be taken carefully into account when normalizing the ED reflectivity data.

The samples were prepared using liquid Ga (99.9% purity, ABCR metals) and a mixture of that liquid Ga and Hg (99.999% purity, Aldrich Chemicals). For each oxidation temperature, a new alloy was mixed to check the consistency of the results. Samples of 40 wt% Hg, 66 wt% Hg and 60 wt% Hg were prepared for the measurements at 83 °C, 107.5 °C and 122 °C, respectively. All of the mixtures are clearly situated in the miscibility gap of Ga–Hg, therefore giving rise to a two-phase separation where a Ga-rich phase forms a homogeneous layer on top of a Hg-rich phase. According to the phase diagram, the atomic composition of the Ga-rich phase is Ga_xHg_{1-x} with $x = 0.94$, 0.93 and 0.92 for $T = 83$, 107.5 and 122 °C, respectively [11]. However, with regard to the accuracy of the phase diagram, it seems appropriate to refer to a nearly constant alloy composition of $x = 0.93 \pm 0.01$ for the temperatures studied.

The samples were inserted into a stainless steel trough within a furnace chamber at ambient conditions, forming layers of about 400 μm thickness. Such shallow layers are needed to suppress mechanically excited low-frequency surface waves, which are attenuated by viscous drag at the liquid/trough interface [26], and which otherwise would give rise to resolution losses as they are equivalent to a higher effective curvature [27]. The sample trough was designed with overhanging edges to obtain a liquid surface that is as flat as possible despite the high contact angles of Ga and Hg with stainless steel. The curvature was controlled by an optical Michelson interferometer [27] indicating surface radii of at

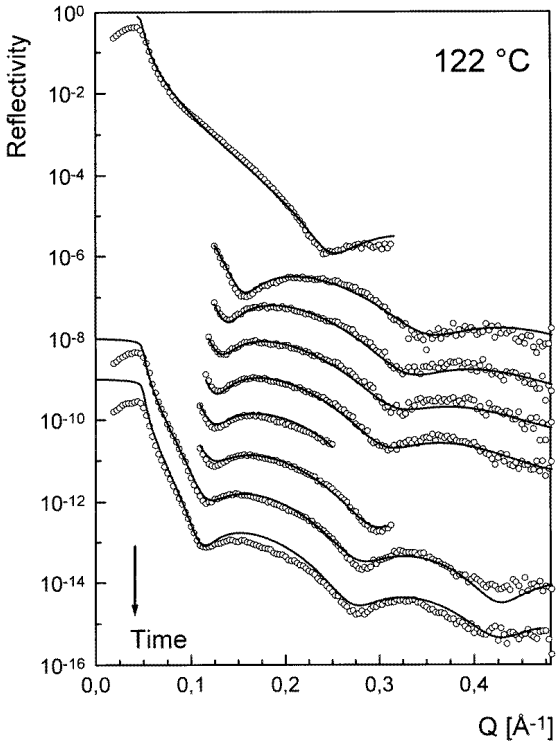

Figure 3. As figure 1, but for $T = 122$ °C.

least 40 metres. Hence, we conclude that the total angular divergence in this experiment, resulting from the sample curvature and the reflectometer optics, could be kept below 0.8 mrad (0.046°), which is a sufficient resolution for studying the extended reflectivity oscillations from oxide layers of even several 100 Å thickness.

After inserting each sample into the trough, an oxide layer was clearly visible, which was carefully stripped off by means of a scalpel, resulting in an optically clean and shining surface. However, since the spontaneous oxidation of liquid Ga surfaces when exposed to oxygen at ambient conditions is well known [12, 14], it was important to characterize the initial oxidation state of the samples. Therefore, a reflectivity curve was measured after sweeping the surface, prior to rapid heating to the selected temperatures. The beginning of the rapid heating (which took approximately 20 minutes until the thermal equilibrium was reached) was defined as a reference time t_0 for the subsequent observation of the oxidation process. The relatively quick initial growth of the oxide layers after t_0 was monitored by fast ED scans of about 20 minutes duration, marking the time resolution of the experiment. For later times with lower growth rates the reflectivity measurements were expanded to the whole accessible Q-range by performing fast AD scans in the total reflection regime and collecting ED spectra at several fixed angles. The data could be overlapped easily when plotted as a function of the momentum transfer Q. Measurements of the incident beam provided absolute units for the reflectivity. The data were corrected for diffuse scattering on the basis of longitudinal offset scans [28], which could be observed in the ED mode by shifting the detector angle to an off-specular position, the offset being 1.5 times the specular beam width.

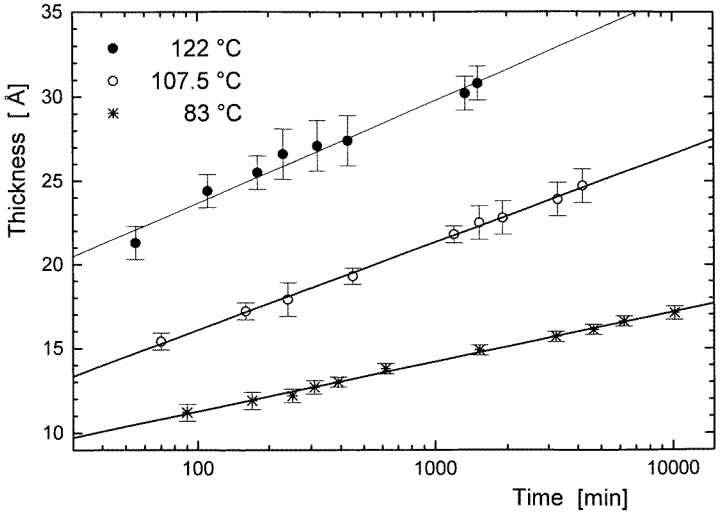

Figure 4. The thickness of the oxide layer on $Ga_{0.93}Hg_{0.07}$ versus time. The time resolution is approximately 20 minutes. Each solid line represents a straight-line fit.

4. Results

4.1. Oxidation of the alloy

Reflectivity data for the oxidation of the alloy at different temperatures are shown in figures 1–3 together with box model fits, where the oxide layer is represented by a box of constant electron density.

The topmost curves in each figure show the reflectivity at ambient conditions before rapid heating. The intensity minimum at $Q = 0.22$–0.33 Å^{-1} is due to an extended thickness oscillation, indicating the presence of a thin native oxide layer at room temperature. The thickness of these oxide layers was found by simulation to range from 8 to 12 Å, depending on the sample investigated. All of the reflectivity data are reproduced well by fits assuming only a single oxide layer of constant density (the one-box model), which we found useful to characterize the samples with a minimum of parameters. However, there are some differences between data and simulation in the high-Q part of figure 2, which hint at a graded density profile of the initial oxide layer on that sample. The fits yield rather low oxide densities of 2.0 ± 0.4 g cm^{-3}. The chemical composition of the oxide layer was assumed to be Ga_2O_3 since this oxide forms naturally on liquid Ga in air [29]. In addition, the fluorescence and absorption structure of ED spectra provided no evidence for significant incorporation of Hg into the layer.

The data below the topmost curves in figures 1–3 were obtained after heating to the temperature displayed in the figure. Reflectivities starting at $Q \approx 0.125$ Å^{-1} indicate fast ED measurements, whereas data containing the total reflection regime are overlapped AD and ED measurements (see the previous section). Even without detailed analysis, the experimental data clearly indicate a growing oxide layer, evident from the shift of the intensity minimum to lower Q-values.

Solid lines in figures 1–3 represent fits to the experimental data. The discrepancies between the measured data and simulated reflectivities below the total reflection edge are due to the large footprint of the x-ray beam on the curved sample at extremely grazing

angles, resulting in a divergent reflected beam that cannot be received fully by the detector aperture. For all of the simulations the oxide was idealized as a single layer of constant density. Even though this is probably an oversimplification, we feel that the data are more adequately described by this model, especially as very thin oxide layers give rise to quite extended reflectivity oscillations which were only observable in our experiment up to $Q \approx 0.4$ Å^{-1}.

Within this approximation, the density of the oxide (assuming again Ga_2O_3) could be determined to 3.4 ± 0.2 g cm^{-3}, in remarkable contrast to the density of the layer present at room temperature. The surface and interface roughness seem to change only slightly, if at all, during the growth process, as is evident from the observation of a constant level of non-specular scattering. This is in agreement with nearly constant RMS roughness parameters, remaining between 4 and 6 Å for all of the fits.

Figure 4 shows the oxide layer thickness extracted from the single-layer model for different times. For each temperature, the layer thicknesses grow significantly with time. Within experimental error, the growth behaviour is well described by a logarithmic growth law $X \propto \ln t$, where X denotes the oxide thickness. As expected for a temperature-activated oxidation process, the oxide thickness increases with temperature, resulting in layers ranging from 20–30 Å at 122 °C compared to 12–17 Å at 83 °C.

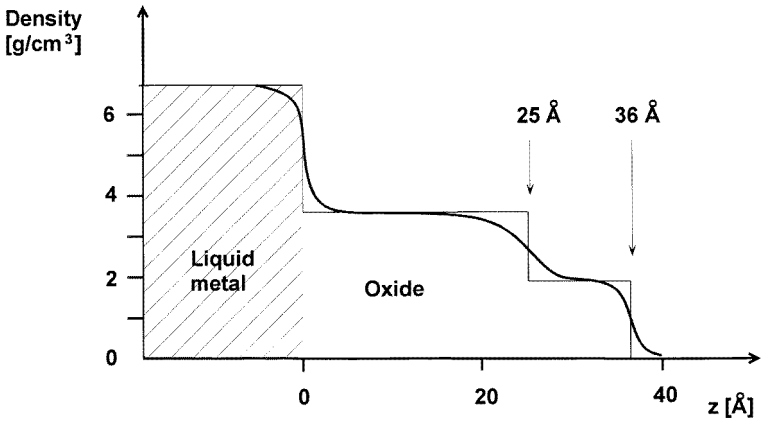

Figure 5. The box model for the simulation of reflectivity curves for thicker oxide layers (example: $Ga_{0.93}Hg_{0.07}$ oxidized for 1520 minutes at 122 °C). Z denotes the height above the liquid metal–oxide interface. The full line shows the density profile after the inclusion of surface and interface roughness.

How accurately does the single-layer model describe the data? It is interesting to note that the thicker oxide films found for $T = 122$ °C give rise to two observable oscillations that warrant a fit with a two-layer model. Such 'bilayer' fits were carried out for a few reflectivity curves, improving the single-layer fits moderately and resulting in a light layer at the air/oxide interface together with a denser layer at the oxide/liquid metal interface as sketched in figure 5. The time dependence seems to indicate a light top layer of constant thickness, whereas the denser layer beneath showed growth behaviour. Although it is tempting to speculate that the top layer corresponds to the natural oxide layer grown at room temperature, it must be kept in mind that these results could also simply represent oxide films with a continuously graded density profile, approximated by a bilayer. However, since the reflectivity data for $T = 122$ °C could essentially be fitted with the single-layer

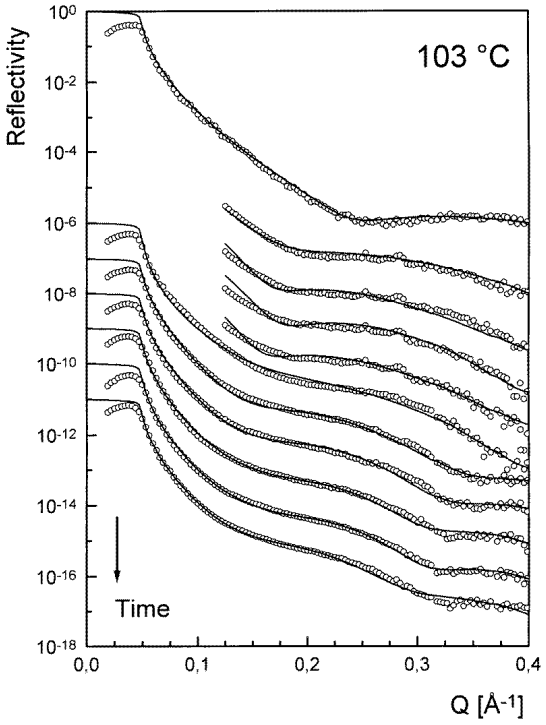

Figure 6. Reflectivities observed for the oxidation of liquid Ga at $T = 103$ °C. The data and fits are displayed as in figures 1–3.

model, it seemed therefore most appropriate to use only this model to analyse the growth behaviour at all temperatures on the same footing.

4.2. Ga oxidation

Liquid Ga has been oxidized at $T = 103$ °C for comparison. The experimental data and fits are shown in figure 6. The oxide growth is very similar to that observed for $Ga_{0.93}Hg_{0.07}$; however, we found an increased oxide density of 4.5 ± 0.2 g cm^{-3}. Due to the smaller electron contrast with the underlying liquid Ga, this leads to reflectivity curves with clearly reduced oscillation amplitudes, giving rise to a larger thickness error. Nevertheless, the thickness of the oxide on liquid Ga clearly exceeds that on $Ga_{0.93}Hg_{0.07}$, although following a similar logarithmic growth law as shown in figure 7.

5. Discussion

5.1. Structural aspects

The well-defined interference pattern shown by the reflectivity curves clearly demonstrates the presence of a surface oxide film of uniform thickness, which must extend over almost the complete illuminated area on the sample (15 mm $\times$ 4 mm). This is consistent with observations of Chabala [12] and Wang *et al* [13] who conclude that the oxide formation on liquid Ga proceeds by aggregation of isolated oxide clusters which eventually form a closed

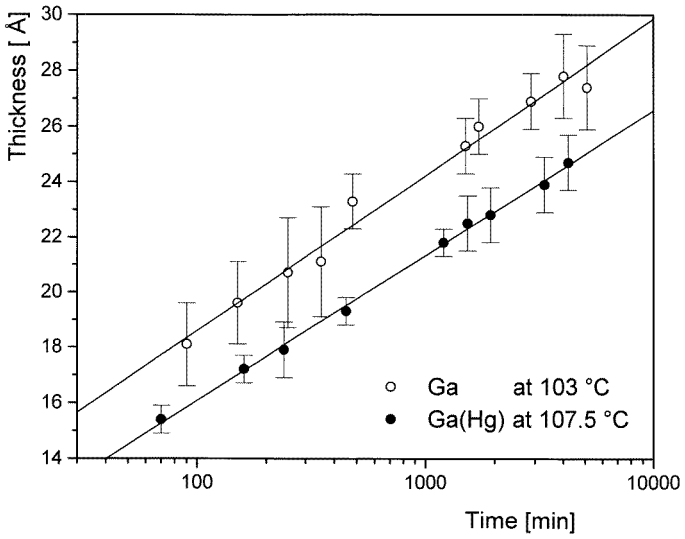

Figure 7. Oxide film growth on liquid Ga compared to that on $Ga_{0.93}Hg_{0.07}$ at similar temperatures. The solid lines are a guide to the eye.

thin porous film. Since they find an exponential growth of the average cluster size with time and characteristic oxygen exposures of several hundreds of langmuirs (1 L $= 10^{-6}$ Torr s for oxygen) for a full coverage of the underlying liquid, oxidation in air at STP should result in an essentially spontaneous ($t < 10^{-5}$ s) oxide film, which was observed here as the starting point of the experiment. However, the estimate of Wang *et al* for the film thickness at room temperature is of the order of 100 Å, which is in remarkable contrast to our results, indicating approximately 10 Å. Since their estimate was rather indirectly inferred from the ion beam current and an assumed yield of their sputtering experiment, whereas x-ray reflectivity oscillations are directly related to the film thickness, we consider our results more reliable. In addition, Chabala's SIMS measurements also indicated an oxide film a few monolayers thick, in agreement with our results. Nevertheless, the conclusion of a porous film is fully corroborated and quantified by the oxide densities derived from our simulations. In spite of the considerable error margin, the room temperature oxide density of 2.0 ± 0.4 g cm^{-3} differs substantially from the bulk density of 5.88 g cm^{-3} for β-Ga_2O_3 [30], which is most naturally explained by a loosely packed and/or porous oxide structure.

It is interesting to note that the reflectivity data obtained at higher temperatures (83–122 °C) are best fitted with an enhanced density of 3.4 ± 0.2 g cm^{-3}, which might be attributed to a more compact oxide structure due to increased thermally activated migration; nevertheless this density still implies a porous film.

In a recent study, Regan *et al* [15] exposed liquid Ga surfaces to controlled oxygen dosages up to 1600 L under ultrahigh-vacuum (UHV) conditions. They report the formation of a 5 Å oxide film, covering the underlying liquid at dosages as low as 200 L, and conclude furthermore that the oxide layer is probably a poorly crystallized or amorphous solid. This finding is supported by our observation of distinct thickness oscillations in longitudinal offset scans (not shown here). It is well known that correlated interface roughness gives rise to a diffuse background modulated with the same periodicity as the specular curve [28]. Since a static roughness correlation of the two interfaces is very likely to arise for a thin solid film and, additionally, the RMS roughness of liquid interfaces usually turns out to be

less than 1 Å [15], whereas we find here 4–6 Å, it is reasonable to suppose that solid oxide layers were observed here, too.

5.2. Growth kinetics

The oxide growth on both liquid Ga and $Ga_{0.93}Hg_{0.07}$ is in good agreement with logarithmic kinetics, which is a common phenomenon for thin oxide layers and low oxidation temperatures [5, 31–33]. Several theories for logarithmic growth have been worked out, which are in general based on a differential equation of the form [5, 32]

$$\frac{dX}{dt} = \alpha \exp(-\beta X) \tag{3}$$

where X denotes the oxide thickness and t the oxidation time. α and β are defined by

$$\alpha = A \exp(-E/kT) \tag{4}$$

$$\beta = B/kT \tag{5}$$

where T denotes the absolute temperature, k the Boltzmann constant, A and B describe oxide properties and E is a characteristic energy. Integration of equation (3) yields a logarithmic time law:

$$X = \frac{1}{\beta} \ln(\alpha\beta t + 1). \tag{6}$$

As is evident in figures 4 and 7, the time dependence of the oxide layer thickness (extracted from the single-layer model) is well described in all cases by a direct logarithmic law, corresponding to $\alpha\beta t \gg 1$. No correction has been applied to account for the thickness of the initial oxide layer that had already formed at room temperature. However, as this layer forms within fractions of a millisecond, this corresponds in essence to an error in the determination of the oxidation time which is irrelevant compared to the error of t_0 (see section 3).

Our finding of logarithmic growth is at variance with observations by Regan *et al*, who reported a *saturation* thickness of 5 Å for an oxide layer on liquid Ga for oxygen exposures exceeding 400 L [15]. However, it must be emphasized that we investigated the growth of a natural oxide in air, whereas Regan *et al* used a controlled oxygen dosage under UHV conditions. In addition, the influence of cracks in the oxide film and the presence of other chemical species (e.g. nitrogen) on the detailed oxidation behaviour is not well understood at present. Clearly, further investigations are needed to clarify this point.

The temperature-dependent oxidation data for $Ga_{0.93}Hg_{0.07}$ allow us to assess the activation energy E of the oxidation process. If electron transport is the rate-limiting step for oxide formation, which is a sensible assumption for oxide layers below 40 Å [3], a logarithmic growth law can be derived where E describes the energy for electron escape from the metal [5]. Since this theory reproduces also the empirical Rideal–Wansbrough-Jones relation [34] $E = \phi - K$, where ϕ is the metal work function and $K = 3.6$ eV is a constant related to the electron affinity of oxygen, the measured activation energy can be cross-checked with tabulated work-function data.

The analysis of our data gives an activation energy $E = 1.0 \pm 0.7$ eV, the error being mainly due to the uncertainty in the starting time t_0. As the work function of $Ga_{0.93}Hg_{0.07}$ is not known, the value $\phi = 4.12$ eV for Ga [35] was used instead to calculate an estimated activation energy of $E \approx 0.5$ eV, which is in agreement with our result. However, the admittedly large error of E might also mask a significant difference of the respective work functions for liquid Ga and $Ga_{0.93}Hg_{0.07}$, since a higher activation energy for the oxidation

of the alloy might be responsible for the lower thicknesses of oxide as compared to Ga as shown in figure 7.

In view of the saturation thickness observed by Regan *et al*, we have also checked whether our data can be explained by the Mott–Cabrera (MC) theory of low-temperature oxidation, which is usually associated with the concepts of a limiting oxide thickness and an inverse-logarithmic growth law [4]. However, since Ghez has shown that the inverse-logarithmic law is not even an asymptotic solution of the MC rate equation, we analysed our data using his more accurate treatment [36]. As these attempts led to negative activation energies, the MC theory can thus be excluded from consideration as a description of our results.

6. Conclusion

It has been shown that x-ray reflectivity is a technique that is also well suited for monitoring the growth of very thin oxide layers on liquid substrates. Due to the large footprint of the x-ray beam in grazing-incidence geometry, a large representative area was sampled in these experiments. The combination of AD and ED measurements allowed us to obtain absolute reflectivity units and to achieve fast data collection up to $Q = 0.5$ Å^{-1} with a sealed-tube reflectometer.

We found a logarithmic growth law for the oxidation of liquid Ga and $Ga_{0.93}Hg_{0.07}$, thus demonstrating explicitly that logarithmic growth behaviour can already be observed for ultrathin oxide films well below 40 Å. The activation energy for the oxidation of $Ga_{0.93}Hg_{0.07}$ was assessed and found to be in agreement with the Rideal–Wansbrough-Jones prediction following also from Uhlig's derivation of a logarithmic time law, whereas the data could not be described by the Mott–Cabrera theory.

In future work, extension of these measurements would clearly benefit from UHV chambers and the use of intense synchrotron radiation, allowing the study of oxidation kinetics on much shorter timescales and the determination of precise activation energies. We are currently planning such experiments.

References

[1] Wagner C 1933 *Z. Phys. Chem.* B **21** 25
[2] Mott N F 1939 *Trans. Faraday Soc.* **35** 1175
[3] Mott N F 1947 *Trans. Faraday Soc.* **43** 431
[4] Cabrera N and Mott N F 1949 *Rep. Prog. Phys.* **12** 163
[5] Uhlig H H 1956 *Acta Metall.* **4** 541
[6] Fromhold A T Jr and Cook E L 1966 *Phys. Rev. Lett.* **17** 1212
[7] Fromhold A T Jr and Cook E L 1967 *Phys. Rev.* **158** 600
Fromhold A T Jr and Cook E L 1967 *Phys. Rev.* **163** 650
[8] Salas O, Jayaram V, Vlach K, Levi C G and Mehrabian R 1995 *J. Am. Ceram. Soc.* **78** 609
[9] Stoneman A M and MacKay C A 1980 *Metallurgica* **34** 49
[10] Preuss A, Adolphi B and Wegener T 1995 *Fresenius J. Anal. Chem.* **353** 399
[11] Predel B 1960 *Z. Phys. Chem.* **24** 206
[12] Chabala J M 1992 *Phys. Rev.* B **46** 11 346
[13] Wang Y L, Doong Y Y, Chen T S and Haung J S 1994 *J. Vac. Sci. Technol.* A **12** 2081
[14] Wang Y L and Lin S J 1996 *Phys. Rev.* B **53** 6152
[15] Regan M J, Tostmann H, Pershan P S, Magnussen O M, DiMasi E, Ocko B M and Deutsch M 1997 *Phys. Rev.* B **55** 10 786
[16] Leibbrandt G W R, Hoogers G and Habraken F H P M 1992 *Phys. Rev. Lett.* **68** 1947
[17] Russell T P 1990 *Mater. Sci. Rep.* **5** 171
[18] Als-Nielsen J, Jacquemain D, Kjaer K, Leveiller F, Lahav M and Leiserowitz L 1994 *Phys. Rep.* **246** 251

[19] Stierle A, Mühge T and Zabel H 1994 *J. Mater. Res.* **9** 884
[20] James R W 1962 *The Optical Principles of the Diffraction of X-rays* (Woodbridge, CT: Ox Bow)
[21] Stanglmeier F, Lengeler B, Weber W, Göbel H and Schuster M 1992 *Acta Crystallogr.* A **48** 626
[22] Pershan P S and Als-Nielsen J 1984 *Phys. Rev. Lett.* **52** 759
[23] Parratt L G 1954 *Phys. Rev.* **95** 359
[24] Névot L and Croce P 1980 *Revue Phys. Appl.* **15** 761
[25] Metzger T H, Luidl C, Pietsch U and Vierl U 1994 *Nucl. Instrum. Methods* A **350** 398
[26] Pershan P S 1990 *Faraday Discuss. Chem. Soc.* **89** 231
[27] Bridou F 1994 *J. Physique* III **4** 1513
[28] Sinha S K, Sirota E B, Garoff S and Stanley H B 1988 *Phys. Rev.* B **38** 2297
[29] Su C Y, Skeath P R, Lindau I and Spicer W E 1982 *Surf. Sci.* **118** 248
[30] *CRC Handbook of Chemistry and Physics* 1991 ed D R Lide, 72nd edn (Boca Raton, FL: Chemical Rubber Company Press)
[31] Tammann G and Köster W 1922 *Z. Anorg. Allg. Chem.* **123** 196
[32] Konetzki R A and Chang Y A 1989 *J. Mater. Res.* **4** 1421
[33] Martin M, Mader W and Fromm E 1994 *Thin Solid Films* **250** 61
[34] Rideal E and Wansbrough-Jones O 1929 *Proc. R. Soc.* A **123** 202
[35] *Landolt–Börnstein New Series* 1955 Group II, vol 4 (Berlin: Springer)
[36] Ghez R 1973 *J. Chem. Phys.* **58** 1838